Phonon dispersion in the one-layer cuprate $HgBa_2CuO_{4+\delta}$

2003 J. Phys.: Condens. Matter 15 8827

(http://iopscience.iop.org/0953-8984/15/50/014)

INSTITUTE OF PHYSICS PUBLISHING JOURNAL OF PHYSICS: CONDENSED MATTER

J. Phys.: Condens. Matter **15** (2003) 8827–8836 PII: S0953-8984(03)69695-5

Phonon dispersion in the one-layer cuprate $HgBa_2CuO_{4+\delta}$

Matteo d'Astuto[1,3], Alessandro Mirone[1], Paola Giura[1], Dorothée Colson[2], Anne Forget[2] and Michael Krisch[1]

[1] European Synchrotron Radiation Facility, BP 220, F-38043 Grenoble Cedex, France
[2] Service de Physique de l'Etat Condensé, CEA Saclay, F-91191 Gif-sur-Yvette Cedex, France

E-mail: matteo.dastuto@pmc.jussieu.fr

Received 24 September 2003
Published 3 December 2003
Online at stacks.iop.org/JPhysCM/15/8827

Abstract

We investigate the low energy acoustical and optical modes in $HgBa_2CuO_{4+\delta}$ using inelastic x-ray scattering (IXS). The experimental phonon dispersion and the dynamical structure factor are compared with an atomic shell model, and the set of atomic potentials obtained is discussed. Our results are also compared with those obtained by Raman spectroscopy and with density-of-state data measured by inelastic neutron scattering.

1. Introduction

The cuprate family of $HgBa_2Ca_{n-1}Cu_nO_{2n+2+\delta}$ (or Hg-12$(n-1)n$) has the highest known superconducting transition temperature at ambient pressure, with a T_c of 136 K for the three-layer compound $HgBa_2Ca_2Cu_3O_{8+\delta}$ (Hg-1223) (Putilin *et al* 1993, Schilling *et al* 1993). Moreover, its superconducting gap shows a peculiar symmetry, different from the $d_{x^2-y^2}$ symmetry found in the majority of the other cuprates, as Sacuto *et al* (1997) clearly proved for $HgBa_2CaCu_2O_{6+\delta}$ (Hg-1212). Within this family, $HgBa_2CuO_{4+\delta}$ (Hg-1201) is perhaps even more intriguing, being the one-layer hole doped cuprate with the highest superconducting transition temperature $T_c = 97$ K, more than twice those of the other one-layer cuprates (25 K–40 K). At the same time it presents one of the simplest crystal structures, a tetragonal primitive $P/4mmm$ (see figure 1) symmetry, with very few impurities, no distortions and almost perfect square Cu–O_2 planes (Bertinotti *et al* 1997). For these reasons, Hg-1201 is considered as a prototype among the superconductor cuprates and relevant information on the origin and on the detailed microscopic mechanism of the superconductivity is expected from the study of the collective excitation dynamics (electronic, crystalline, e.g. phonons, and

[3] Present address: Physique des Milieux Condensés, Université Pierre et Marie Curie, CNRS UMR 76 02, F-75252 Paris Cedex 05, France.

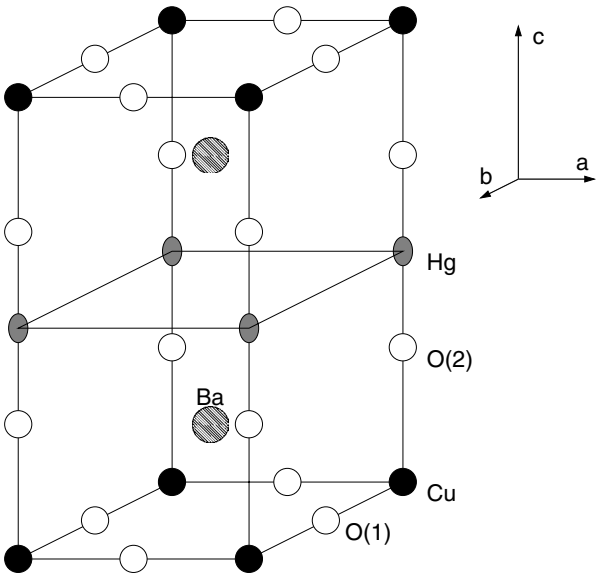

Figure 1. Crystal structure of $HgBa_2CuO_{4+\delta}$. O(1), *in-plane* oxygen; O(2), *out-of-plane* oxygen; $a = b = 3.874(1)$ Å; $c = 9.504(9)$ Å; zO(2) $= 0.2092(6)$ rlu; zBa $= 0.2.991(1)$ rlu (Bertinotti *et al* 1996).

magnetic[4]) of this system. However, such a kind of study is experimentally not trivial since the synthesis of superconducting Hg-1201 single crystals is possible only for volumes smaller than 0.1 mm^3 (see Bertinotti *et al* 1997). Such a size is insufficient for inelastic neutron scattering (INS), that is the standard technique used to measure the dispersion of phonons. For this reason, phonon data on this system were, up to now, limited to the ones obtained by INS performed on powders, which gives a measure of the phonon density of state (PDOS) (Renker *et al* 1996), and by Raman spectroscopy (Hur *et al* 1993, Krantz *et al* 1994, Lee *et al* 1994, Ren *et al* 1994, Yang *et al* 1995, Zhou *et al* 1996a, 1996b, Poulakis *et al* 1999 and Cai *et al* 2001). These experimental results have been analysed using a shell model calculation by Renker *et al* (1996) and Stachiotti *et al* (1995), who have also determined the zone centre frequencies from frozen-phonon first principles calculations.

Nowadays, the study of the phonon dispersion in sub-millimetre size cuprate crystals is possible by means of inelastic x-ray scattering (IXS), as shown by d'Astuto *et al* (2002, 2003), and, very recently, by Fukuda *et al* (2003). Nevertheless, the measurements of phonons by IXS still represent a difficult task, since the relevant scattering cross section, $\propto f(Q)^2 \propto Z^2$, is due to the oxygen motion, while the relevant penetration depth, $\propto \frac{1}{Z^4}$, is dominated by the high Z ions (neodymium in d'Astuto *et al* (2002, 2003) or mercury and barium in the present work), a fact that strongly reduces the scattering volume. Moreover, the tails of the elastic as well as the low energy phonon lines, to which all the atoms contribute, rise the background under the weaker high energy phonons. For further detail see d'Astuto *et al* (2003). Nevertheless, despite these experimental difficulties, Hg-1201 still remains, thanks to its simple structure, one of the

[4] For a full discussion of the superconductivity in cuprates and the role of the different collective excitations in these systems we refer the reader to the reviews by Orenstein and Millis (2000), Hussey (2002) and Moriya and Ueda (2003), while for a discussion of the role of phonons in cuprates to Pintschovius and Reichardt (1998) as well as the recent works of Anderson (2002), Bohnen *et al* (2002), Chung *et al* (2003) and Bishop *et al* (2003) and references therein.

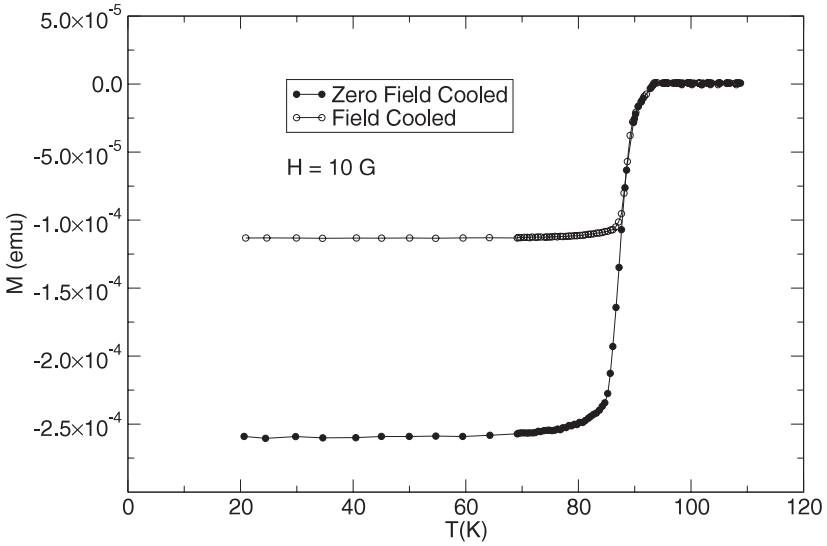

Figure 2. Magnetization as a function of temperature for the sample used in the present experiment.

most suitable systems for the understanding of the phonon dispersion and consequently of the effects of the electron–phonon coupling.

In this first investigation, we focus the analysis on the Hg-1201 low energy acoustical and optical modes, both in longitudinal and transverse polarization. Particular attention is dedicated to the calculation of the dispersion of the transverse acoustic modes, in order to establish an accurate theoretical model able to predict the energy position and the intensity of the phonons along the dispersion curve. A careful estimation of the dynamical structure factor is, indeed, fundamental to select the optimal Brillouin zone which maximizes the intensity of the high energy modes that scatter weakly the x-rays, as well as to assign the correct character to the observed branches.

2. Experiment

2.1. Samples

The single crystals of Hg-1201 were successfully grown by the flux method. The procedure for crystal growth will be described elsewhere (Colson *et al* 2003). The sample size is about $1 \times 1 \times 0.1$ mm^3, with the shorter size along the c-axis. The sample is as grown, with no annealing process, in order to have the best crystalline quality: the typical mosaic spread around the a-direction is about 0.03°. As the sample is as grown, the superconducting transition is not sharp, but spread out over a temperature range of $\Delta T \simeq 5$ K (90% T_c–10% T_c), as shown in figure 2, with a nearly optimal T_c onset of about 94 K.

2.2. Inelastic x-ray scattering

The IXS measurements were carried out on the undulator beam-line ID28 at the European Synchrotron Radiation Facility, Grenoble. The incident beam is monochromatized by a perfect plane Si crystal (Verbeni *et al* 1996), working in extreme backscattering geometry at the

(9, 9, 9) reflection (17 794 eV), with ≈0.7 THz resolution and a wavelength $\lambda = 0.6968$ Å, and at the (8, 8, 8) reflection (15 817 eV) with ≈1.3 THz resolution, high flux and a wavelength $\lambda = 0.7839$ Å. The monochromatic beam is focused onto the sample position by a toroidal mirror in a 250×90 μm^2 spot. The scattered photons are analysed by a bench of five spherically bent high resolution Si analysers (Masciovecchio *et al* 1996a, 1996b), placed on a 7 m long horizontal arm. The analysers are held next to one another with a constant angular offset of about 1.5° and operate in backscattering geometry at the same reflection order as the monochromator. The sample was kept at ambient temperature in a vacuum chamber in order to prevent scattering from air and oxidation of the specimens. The sample chamber is held on a standard diffraction goniometer. The energy ($h\nu$) scans are performed by varying the monochromator temperature while keeping the analyser crystals at a fixed temperature. Further details of the technique can be found in the reviews of Sette *et al* (1996) and Burkel (2000). Krisch *et al* (2002) give a detailed description of the set-up for the ID28 spectrometer at ESRF, as used in the present work.

IXS scans were taken at $Q = G + q$ points of the reciprocal lattice, where G is the zone centre vector, and q is the reduced vector which corresponds to the phonon propagation vector. Longitudinal or (*quasi*-)transverse phonon polarization can be selected according to the relative direction of q and Q: parallel for longitudinal scans or (nearly) perpendicular in the second case.

2.3. Data analysis

The energy scans are fitted using a sum of pseudo-Voigt functions:

$$I\left((1-\eta)\frac{\Gamma^2}{(\epsilon-\epsilon_0)^2+\Gamma^2}+\eta\exp\left(-\frac{(\ln 2)(\epsilon-\epsilon_0)^2}{\Gamma^2}\right)\right) \tag{1}$$

where $\epsilon = \hbar\omega = h\nu$ is the energy, for both the elastic and the inelastic contributions. The half width at half maximum (HWHM) Γ is fixed to the value obtained from a fit of the elastic line due to diffuse scattering. The instrumental line-shape parameter η was taken from a fit to IXS data of nitrogen (Cunsolo *et al* 2003) at $Q \approx 1.9$ Å^{-1}, $P = 0.25$ bar and $T = 66.4$ K, where the diffusion is purely elastic as established by Carneiro and McTague (1975). The line shape described above is in excellent agreement with the instrumental line-shape as can be seen from the elastic signal fit in the energy scans of figure 3. The position ϵ_0 and intensity I of this model are fitted to the *IXS* signal from the phonons of the $HgBa_2CuO_{4+\delta}$ crystals using a χ^2-minimization routine (James and Roos 1975a, 1975b), with the condition that the detailed balance between Stokes and anti-Stokes excitations is fulfilled. A constant background, coming essentially from electronic noise, is added.

2.4. Numerical modelling

Phonon mode frequencies and related atomic displacements were obtained from the diagonalization of the dynamical matrix of a classical shell model with atomic potentials, including screened Coulomb interactions. The matrix was built and diagonalized using the *OpenPhonon* code (Mirone 2003, Mirone and d'Astuto 2003), as in d'Astuto *et al* (2002, 2003).

The PDOS is constructed as a 200-point histogram, whose frequency coordinates range from zero up to the maximum eigen-frequency of the system. The histogram bins are filled calculating the eigen-frequencies over the Brillouin zone on a $11 \times 11 \times 11$ grid. Symmetries are used to reduce the number of necessary calculations. To get the partial DOS for a given site group, the contributions are weighted when added on a particular bin. The weight is calculated

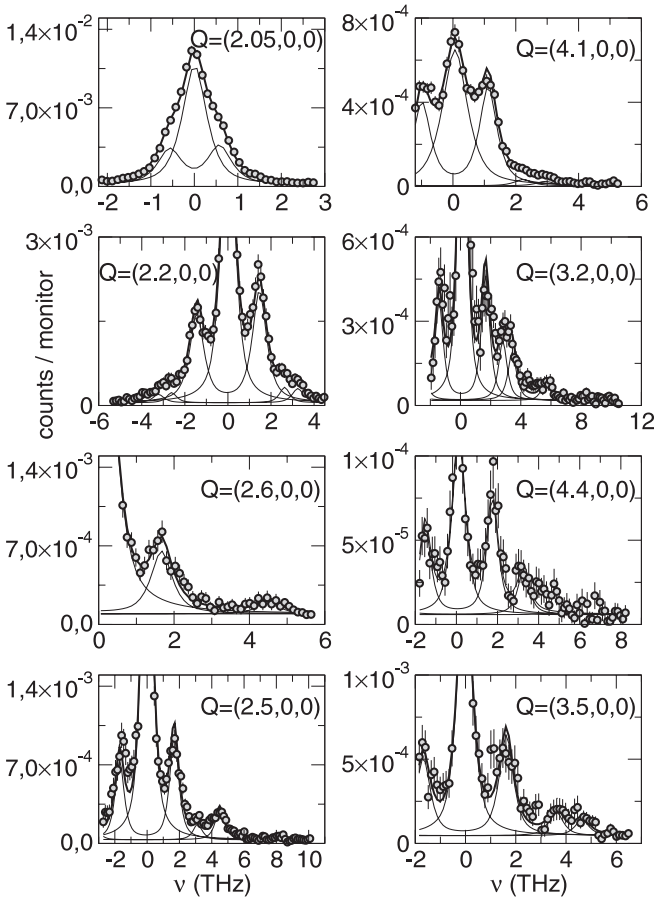

Figure 3. Typical inelastic x-ray scattering (IXS) scans of $HgBa_2CuO_{4+\delta}$ at different scattering vectors, with ∼0.7 THz frequency resolution, normalized to the incident photon flux on an arbitrary scale, and curves corresponding to the best fit using the model as explained in section 2. All data have been collected at room temperature in longitudinal configuration (see the text) parallel to the $a*$-axes, with $Q = G + q = (H, 0, 0) + (\xi, 0, 0)$. Left-hand side: scans in the third Brillouin zone, with $H = 2$ and ξ between 0.05 and 0.5. Right-hand side: scans at higher Q, in the fourth and fifth zone, with $H = 3$ and 4. In the second and the fourth row of the figure, each pair of graphs correspond to the same reduced q vector, with $\xi = 0.2$ and 0.5.

as the modulus square of the eigenvector projection over the considered degrees of freedom (Mirone 2003, Mirone and d'Astuto 2003).

3. Results

Figure 3 reports some representative IXS scans in Hg-1201. Each graph corresponds to a different scattering vector, in two different Brillouin zones. Every scan shows a central peak, at zero frequency, due to the elastic diffuse scattering, and one or more pairs of peaks due to the inelastic scattering from phonons, corresponding to the Stokes and anti-Stokes components of each mode. Note that some scattering vectors correspond to the same reduced reciprocal lattice vector in two different Brillouin zones, showing the variation in intensity due to the change in the dynamical structure factor. The inelastic curves with the greater intensity are

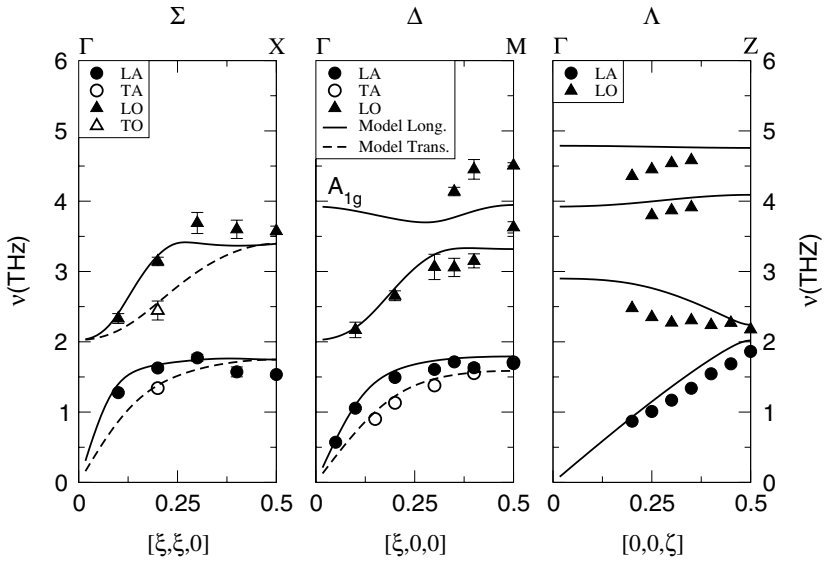

Figure 4. Phonon dispersion in $HgBa_2CuO_{4+\delta}$, along the main symmetry directions with the reduced vector *in plane* ([ξ, 0, 0] and [ξ, ξ, 0]), and perpendicular to the a^*b^* plane [0, 0, ζ]. Symbols represent the experimental frequencies determined from the IXS data as described in the text; continuous curves correspond to the calculated dispersion (see section 3 and table 1).

usually well resolved, with the exception of the scan at $Q = (2.05, 0, 0)$, where the inelastic contribution is too close to the elastic one, resulting in a pair of shoulders on both sides of the elastic curve.

The variation of the frequencies of the phonon modes with the reduced scattering vector q, obtained by the IXS scans as described above, is shown in figure 4, for the main symmetry direction *in plane* (Σ and Δ) and along c^* (Λ). The two highest optic branches along Λ (right-hand panel of figure 4), whose energy separation is less than the experimental resolution, have been measured in separate scans performed in two different Brillouin zones, according to the calculated intensities. Here we also show the calculated dispersion with the empirical model previously described, obtained using the set of atomic potentials reported in table 1. Note that a degeneracy of the *in-plane* longitudinal and transverse modes is calculated at the Σ zone boundary, as already reported by Stachiotti *et al* (1995). Within the experimental accuracy, a similar degeneracy appears in the data at the Δ zone boundary.

Most of the parameters of table 1 are in agreement with the values reported by Renker *et al* (1996) and Chaplot *et al* (1995). Nevertheless, some discrepancies have to be mentioned: the Born–Mayer potentials for the Ba–O(1) and Ba–O(2) bonds are different from the Ba–O potential in Chaplot *et al* (1995), with the first radius $r_{\kappa,\kappa'}$ slightly shorter and the second slightly larger, according to Renker *et al* (1996). Using a mercury ion polarizability[5] of 700 N m^{-1}, and a slightly stiffer additional force constant along the Hg–O(2) bond, if compared to the one of Renker *et al* (1996), we found a good agreement with our experimental dispersion. The histogram of the PDOS calculated with the parameters of table 1 is shown in figure 5.

In table 2 the calculated Raman shift frequencies for the four Raman active modes together with the experimental ones as found by Zhou *et al* (1996b) are reported (other Raman measurements, as Krantz *et al* 1994, Lee *et al* 1994, Poulakis *et al* 1999 and Cai *et al* 2001,

[5] Note that this polarizability has the same value as given by Chaplot *et al* (1995) for the barium ion.

Table 1. Atomic Born–von Karman potential parameter for the calculation of the phonon dispersion (figure 4, bottom panel) and density of states (figure 5, bottom panel). For the definition of the potentials see Chaplot *et al* (1995) and Mirone and d'Astuto (2003).

Site (κ)	Z_κ (e)	Y_κ (e)	K_κ (N m^{-1})
Hg	1.22	2	700
Ba	1.69	3	700
Cu	1.64	3	2000
O(1, 2)	−1.56	−3	1800
Interaction ($\kappa - \kappa'$)	**V°_{BM} (eV)**	**$r_{\kappa,\kappa'}$ (Å)**	
Hg–Ba	2000	0.350	
Ba–Cu	2000	0.335	
Hg–O(1)	2000	0.280	
Hg–O(2)	2000	0.280	$F_L = F_T = 40$ (N m^{-1})
Ba–O(1)	2500	0.315	
Ba–O(2)	2500	0.325	
Cu–O(1)	3950	0.228	
Cu–O(2)	460	0.353	
O(i)–O(j) $i, j = 1, 2$	2000	0.284	$V^\circ_{VW} = -100$ (eV Å^6)

Table 2. Comparison between the experimental Raman shift (Zhou *et al* 1996b) and the shell model (table 1) calculation results for some Raman active modes. For a graphical representation and a symmetry analysis of the modes see Stachiotti *et al* (1995) and Zhou *et al* (1996b).

Mode	Exp. (cm^{-1})	Exp. (THz)	Shell model (THz)
A_{1g} O(2)	592	17.75	17.23
E_g O(2)	165	4.95	7.88
A_{1g} Ba	161	4.83	3.92
E_g Ba	76	2.28	2.84

give similar results). Note that the discrepancy between the calculated A_{1g} Ba mode frequency and the experimental Raman value, of about 0.9 THz, is also present if considering our IXS data, as reported in the central panel of figure 4, although the difference in our case is only ∼0.5 THz.

Finally, by looking at figure 6, in which we report an energy scan performed with the low resolution set-up, we note the presence of a weak signal at high frequency. This signal can be assigned to the in-plane oxygen vibrations.

4. Discussion

The main problem arising from the model calculation of this system using atomic potentials is that the transverse acoustic *in-plane* modes are not stable. In order to remove this instability it is necessary to add a force constant, which makes the bond between the mercury atom and the apical oxygen O(2) less soft against both longitudinal and transverse strains. This because, as pointed out by Pintschovius and Reichardt (1998), open structures cannot be stabilized by simple two-body ionic forces, but need the rigidity of covalent bonds. Therefore, we have optimized this force constant parameter in order to leave the other atomic potentials compatible with the common potential model established by Chaplot *et al* (1995). We stress here that we have not performed a fit of the experimental frequencies, given the limited number of data. In the future, a refined model will be given on the base of a more complete set of measurement,

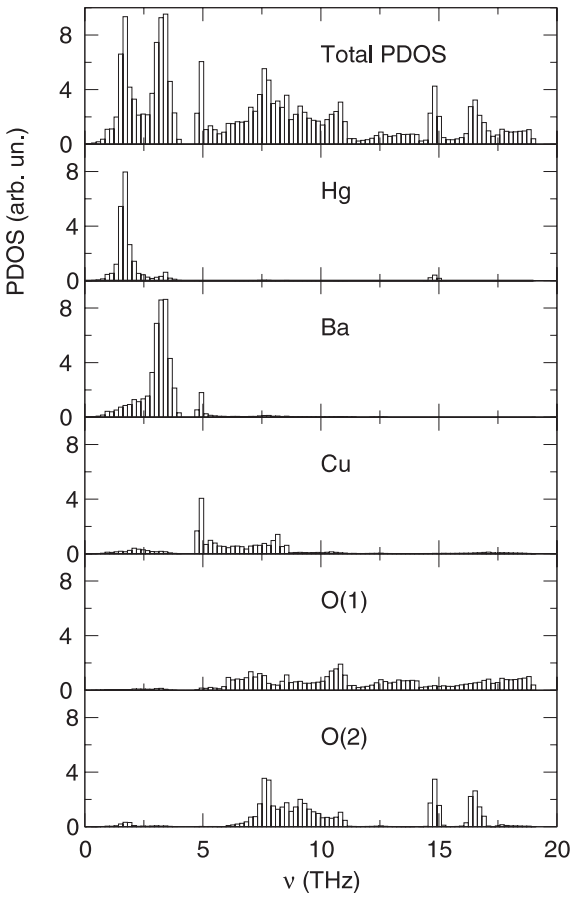

Figure 5. Bar chart of the calculated PDOS.

including at least some of the high frequency modes. For the present purpose we estimate that this accuracy is sufficient.

Concerning the discrepancy with the Raman data, it has to be noted that, first, Zhou *et al* (1996b) express some doubts on the assignment of the signal at 4.83 THz and at 4.95 THz to the two modes A_{1g} Ba and E_g O(2) respectively; second, no direct comparison with the IXS data is possible, since spectra at the zone centre are, in most cases, dominated by strong elastic scattering, masking the weak signal from the optical branches. Therefore, we can only compare the model with IXS results in the whole Brillouin zone but close to Γ, and with Raman results at the zone centre. Further investigation may be necessary, as suggested by Zhou *et al* (1996b), for the correct assignment of the zone centre frequencies.

5. Conclusion

We have presented the first measurements of the phonon dispersion in superconducting Hg-1201. This is an important starting point for further investigations aiming at detecting possible anomalies which can be related to an electron–phonon coupling effect, especially the one concerning the high frequency longitudinal optic mode due to oxygen vibration, as previously observed in other cuprate systems (Fukuda *et al* 2003, Chung *et al* 2003, d'Astuto

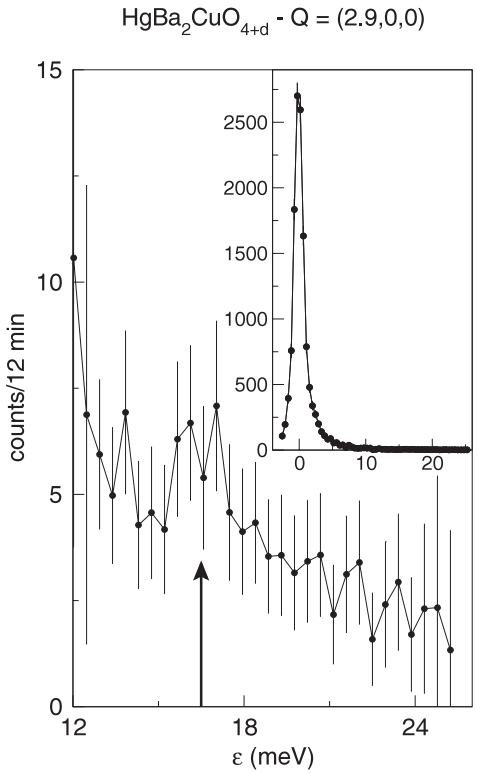

Figure 6. Scan at $Q = (2.9, 0, 0)$, with a resolution of 1.3 THz, using the (888) monochromator reflection.

et al 2002, 2003 and Pintschovius and Reichardt 1998 and references therein). This search is particularly important in the Hg-1201 system as it can be considered as the simplest and most perfect prototype of cuprate superconductors. Further efforts have to be made on the experimental side, using the IXS technique and Raman spectroscopy, which will greatly benefit from the present reference data and which can be guided by the above proposed model. The spectrum in figure 6 is very promising in that sense, also taking into account the recent improvement in the spectrometer efficiency and in the sample growth.

Possible *ab initio* determinations of the phonon dispersion can also be very useful for this purpose, and can be checked against the present set of data.

Acknowledgments

We acknowledge G Monaco for useful discussions and help during the experiments. The authors are grateful to D Gambetti, C Henriquet and R Verbeni for technical help and to J-L Hodeau for his help in the crystal orientation. This work has been supported by the European Synchrotron Radiation Facility (experiment HE-1369).

References

Anderson P W 2002 *Preprint* cond-mat/0201429

Bertinotti A, Colson D, Marucco J-F, Viallet V, Le Bras G, Fruchter L, Marcenat C, Carrington A and Hammann J 1997 Single crystals of mercury based cuprates: growth, structure and physical, properties *Studies of High Temperature Superconductors—Hg-Based High Tc Superconductors* part-I vol 23, ed A Narlikar (New York: Nova) pp 27–85

Bertinotti A, Viallet V, Colson D, Marucco J-F, Hammann J, Forget A and Le Bras G 1996 *Physica* C **268** 257–65
Bishop A R, Mihailovic D and de Leon J M 2003 *J. Phys.: Condens. Matter* **15** L169–75
Bohnen K-P, Heid R and Krauss M 2002 *Preprint* cond-mat/0211084
Burkel E 2000 *Rep. Prog. Phys.* **63** 171–232
Cai Q, Chandresekhar M, Chandrasekhar H R, Venkateswaran U, Liou S H and Li R 2001 *Solid State Commun.* **117** 685–90
Carneiro K and McTague J P 1975 *Phys. Rev.* A **11** 1744
Chaplot S L, Reichardt W, Pintschovius L and Pika N 1995 *Phys. Rev.* B **52** 7230–42
Chung J-H, Egami T, McQueeney R J, Yethiraj M, Arai M, Yokoo T, Petrov Y, Mook H A, Endoh Y, Tajima S, Frost C and Dogan F 2003 *Phys. Rev.* B **67** 014517–9
Colson D *et al* 2003 unpublished
Cunsolo A, Monaco G, Nardone M, Pratesi G and Verbeni R 2003 *Phys. Rev.* B **67** 024507
d'Astuto M, Mang P K, Giura P, Shukla A, Ghigna P, Mirone A, Braden M, Greven M, Krisch M and Sette F 2002 *Phys. Rev. Lett.* **88** 167002
d'Astuto M, Mang P K, Giura P, Shukla A, Mirone A, Krisch M, Sette F, Ghigna P, Braden M and Greven M 2003 *Int. J. Mod. Phys.* B **17** 484–92
Fukuda T, Mizuki J, Ikeuchi K, Fujita M, Yamada K, Baron A Q R, Tsutsui S, Tanaka Y and Endoh Y 2003 *Preprint* cond-mat/0306190
Hur N H, Lee H-G, Park J-H, Shin H-S and Yang I-S 1993 *Physica* C **218** 365–8
Hussey N E 2002 *Adv. Phys.* **51** 1685–771
James F and Roos M 1975a *Comput. Phys. Commun.* **10** 343–67
James F and Roos M 1975b *MINUIT—Function Minimization and Error Analysis—Reference Manual, CERN D506 (Long Writeup)* (Geneva: Computing and Networks Division, CERN) available on line http://cernlib.web.cern.ch/cernlib/
Krantz M, Thomson C, Mattausch H and Cardona M 1994 *Phys. Rev.* B **50** 1165–70
Krisch M, Brand R A, Chernikov M and Ott H R 2002 *Phys. Rev.* B **65** 134201–7
Lee H G, Shin H S, Yang I S, Yu J J and Hur N H 1994 *Physica* C **233** 35–9
Masciovecchio C, Bergmann U, Krisch M, Ruocco G, Sette F and Verbeni R 1996a *Nucl. Instrum. Methods* B **111** 181–6
Masciovecchio C, Bergmann U, Krisch M, Ruocco G, Sette F and Verbeni R 1996b *Nucl. Instrum. Methods* B **117** 339–40
Mirone A 2003 *Open Phonon Code Source, version 3* available on http://www.esrf.fr/computing/scientific/
Mirone A and d'Astuto M 2003 *Open Phonon Manual, version 3* available on http://www.esrf.fr/computing/scientific/
Moriya T and Ueda K 2003 *Rep. Prog. Phys.* **66** 1299–341
Orenstein J and Millis A J 2000 *Science* **288** 468–74
Pintschovius L and Reichardt W 1998 *Neutron Scattering in Layered Copper-Oxide Superconductors* (*Physics and Chemistry of Materials with Low-Dimensional Structures* vol 20) ed A Furrer (Dordrecht: Kluwer) p 165
Poulakis N, Lampakis D, Liarokapis E, Yoshikawa A, Shimoyama J, Kishio K, Peacock G B, Hodges J P, Gameson L, Edwards P P and Panagopoulos C 1999 *Phys. Rev.* B **60** 3244–51
Putilin S N, Antipov E V, Chmaissen O and Marezio M 1993 *Nature* **362** 226–8
Ren Y T, Chang H, Xiong Q, Xue Y Y and Chu C W 1994 *Physica* C **226** 209–15
Renker B, Schober H and Gompf F 1996 *J. Low Temp. Phys.* **105** 843–8
Sacuto A, Combescot R, Bontemps N, Monod P, Viallet V and Colson D 1997 *Europhys. Lett.* **39** 207–12
Schilling A, Cantoni M, Guo J D and Ott H R 1993 *Nature* **363** 56–8
Sette F, Ruocco G, Krisch M, Masciovecchio C and Verbeni R 1996 *Phys. Scr.* T **66** 48–56
Stachiotti M G, Peltzer y Blancá E L, Migoni R L, Rodriguez C O and Christensen N E 1995 *Physica* C **243** 207–13
Verbeni R, Sette F, Krisch M H, Bergmann U, Gorges B, Halcoussis C, Martel K, Masciovecchio C, Ribois J F, Ruocco G and Sinn H 1996 *J. Synchrotron Radiat.* **3** 62–4
Yang I S, Lee H G, Hur N H and Yu J 1995 *Phys. Rev.* B **52** 15078–81
Zhou X J, Cardona M, Chu C W, Lin Q M, Loureiro S M and Marezio M 1996a *Phys. Rev.* B **54** 6137–40
Zhou X J, Cardona M, Chu C W, Lin Q M, Loureiro S M and Marezio M 1996b *Physica* C **270** 193–206